Effects of the Cohesive Law in Ductile Crack Analysis using Cohesive Zone Models

X.Li, H.Yuan[a],

Department of Mechanical Engineering, University of Wuppertal, Wuppertal 42103, Germany

[a]h.yuan@uni-wuppertal.de

Keywords: Cohesive zone model, cohesive law, cohesive element, threshold value, cracking simulation

Abstract. In the present paper effects of cohesive zone models to crack simulation are studied systematically. For this purpose a special cohesive element has been developed and implemented into the commercial FEM code ABAQUS. The computational investigation based on a CT specimen confirms that the load vs. load line displacement curve is slightly dependent on the cohesive zone model. Influence to the fracture parameter, such as δ_5, is limited to 5%. Significant deviation is observed in prediction of crack propagation, the deviation exceeds 35%. To obtain a realistic crack propagation, one has to increase the stiffness of the cohesive zone. The fracture energy release rate from the cohesive zone model computation is generally not equal to the cohesive energy. The difference depends on the cohesive law and vanishes only in an elastic specimen. With increasing cohesive strength, the discrepancy between them grows and becomes stable for $T_{max}>3\sigma_0$ under plane strain loading conditions. The maximum deviation exceeds 40%.

1. Introduction

The cohesive zone model has been popular in computational fracture mechanics community due to its simple formulation, easy implementation in FEM codes and flexible applications in crack analysis. One of key advantages of the model is in separation of material deformations from material failure in a ductile material [1]. The deformation is described by the plasticity and cracking by the cohesive zone model. The fracture process zone is simplified into a strip ahead of the crack tip.

Material behavior in the cohesive zone follows a cohesive law. The cohesive law is responsible for material failure under different loading configuration. The cracking is represented as separation of material which is described by the resistance tractions and the surface separation distance, the $\mathbf{T}$-δ relation defining continuous correlation between traction and separation in the cohesive zone. In general cases both variables are vectors, so that the cohesive law is defined in a vector equation. For a mode I crack, however, only normal traction vs. normal separation plays a role in material failure, that is, the cohesive law is expressed in a function, $T(\delta)$.

Before material damaging, the fracture process zone does not initiate and the cohesive zone should not exist. It follows that the cohesive zone will initiate only the traction ahead of the crack tip exceeds a critical value. The stiffness of the cohesive zone is infinite, *a rigid cohesive zone* [2]. This original idea of the cohesive zone model leads to a discontinuous function $T(\delta)$ and is numerically difficult to handle. The most cohesive laws published papers in the past decades [4-12] prefer to assume a continuous traction-separation relation starting from zero loading. That means, the cohesive zone exists in even without loading, *a soft cohesive zone*.

It is physically meaningless but numerical necessary if one works with the conventional finite element method. It becomes then an open issue how strong the effect of such cohesive laws to cracking simulation is. Numerically this problem becomes how to quantify effects of the material stiffness of the cohesive zone.

Fracture mechanics is built on energy balance around the crack tip and during crack propagation. Using the energy release rate calibrates crack initiation and propagation. In cohesive zone modeling the crack initiates and propagates just based on the energy dissipation in the cohesive zone,

$$\Gamma = \int_0^{\delta_0} T(\delta) d\delta . \qquad (1)$$

Above Γ denotes the cohesive energy to separate a material particle of the cohesive zone. Commonly, the cohesive energy is assumed to equal the energy release rate for fracture [8-11]. Yuan et al. [12] studied variations of the cohesive energy in crack initiation and subsequent crack propagation. It was found that the cohesive energy for crack initiation is significantly larger than Γ for steady-state crack propagation. Computational results [14] show the cohesive energy seems smaller than J_i, almost by factor 2. Based on these observations, it is interesting to re-examine the correlation between the cohesive energy and the energy release rate of fracture.

In the present paper a special cohesive element is developed for analyze effects of the cohesive law. Both discontinuous and continuous cohesive laws can be considered accurately. Interdependence among threshold value of the cohesive laws and the stiffness as well as the maximum strength of the cohesive zone is considered. Finally, the relation between G and J_i is discussed.

2. Formulation of the cohesive element with threshold

Under mode I loading conditions, the crack tip field is symmetric to the crack plane and only a half of the specimen has to be discretized [16]. The cohesive zone initiates and propagates along the symmetric plane. If the cohesive law contains a threshold value, i.e. the cohesive zone initiates only the traction ahead of the crack tip exceeds the threshold value, the conventional continuum element cannot be applied. Since the rigid cohesive zone stiffness before reaching the threshold is infinite, one cannot use the conventional FEM formulation. In the present work only mode I cracks will be considered, so that a crack lies in the symmetric plane and the specimen. One may use the node release technique to simulate crack propagation combined with the cohesive law.

The solid element takes the conventional FEM formulation. The potential cohesive zone is located in the edge of the element. Should the element stress not exceed the threshold value of the cohesive law, the element works as a conventional continuum element. The lower boundary is fixed due to symmetry and enforced to close using the penalty method [17]. As soon as the stress in the element exceeds the threshold value, the node will be released, but loaded by a nodal force and the penalty method for the fixed boundary will be replaced by the cohesive zone. The element surface will not totally release quickly, but loaded by a defined traction which is controlled by the cohesive law. An increment of the cohesive zone is formed. In the following steps the nodal force of the element surface will be release gradually, in accordance with the cohesive law. If the maximum separation is reached, the node is totally free and a crack increment is generated. To improve accuracy of the computations, the stress in the element ahead of the crack tip will be averaged following the idea in [15].

The three-dimensional finite element formulation above has been implemented into the general purpose commercial FEM code, ABAQUS, via the user-defined element (UEL) [18]. Extensive verifications have been taken for the programming. More details about the computational algorithms and programming will be published separately.

3. Cohesive zone models

Cohesive laws have been suggested in most different forms. To study effects of the cohesive laws in ductile failure, the cohesive law with constant maximum traction, T_{max}, is used, as shown in Fig. 2, applied for studying the cohesive zone stiffness effect. The function can be written as,

$$T=\begin{cases} T_{\max}\left(\dfrac{\delta}{\delta_1}\right) & \text{for } \delta \le \delta_1, \\ T_{\max} & \text{for } \delta_1 < \delta \le \delta_2, \\ T_{\max}\left[2\left(\dfrac{\delta-\delta_2}{\delta_0-\delta_2}\right)^3 - 3\left(\dfrac{\delta-\delta_2}{\delta_0-\delta_2}\right)^2 + 1\right] & \text{for } \delta_2 < \delta \le \delta_0. \end{cases} \quad (2)$$

In the cohesive law there are 4 parameters, the maximum traction ,$T_{\max}$; the separation for the initial linear hardening stage, δ_1; the separation for the end of the constant cohesive strength, δ_2, as well as the maximum separation for failure, δ_0. δ_1 is introduced to vary the stiffness of the cohesive zone. The stiffness of the cohesive zone can be quantified by

$$\psi = T_{\max}/\delta_1. \quad (3)$$

Systematic changes of δ_1 lead to various cohesive models. Should δ_1 vanish, the cohesive zone becomes rigid before reaching threshold, i.e. ψ becomes infinite, the cohesive law is discontinuous and contains a threshold value equal $T_{\max}$.

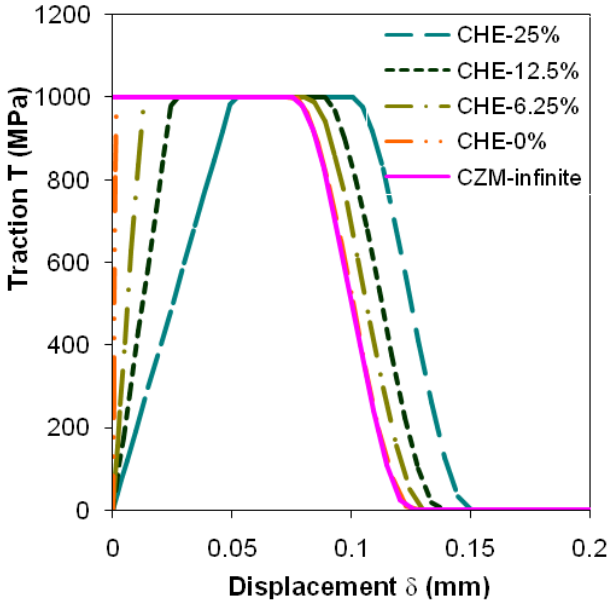

Figure 2. Cohesive laws applied for studying effects of the cohesive zone stiffness. All curves contain the same cohesive energy Γ.

The cohesive energy defined in equation (1) can be re-written as,

$$\Gamma = \frac{1}{2}T_{\max}\delta_1 + T_{\max}(\delta_2-\delta_1) + \frac{1}{2}T_{\max}(\delta_0-\delta_2). \quad (4)$$

The cohesive energy consists of three parts which are defined as,

$$\Gamma = \Gamma_{hd} + \Gamma_{cs} + \Gamma_{sf}. \quad (5)$$

with the cohesive hardening energy denoting the first linear part, the cohesive constant energy for the constant part and the cohesive softening energy for the softening part, respectively, defined as

$$\Gamma_{hd} = \frac{1}{2}T_{\max}\delta_1, \quad \Gamma_{cs} = T_{\max}(\delta_2-\delta_1), \quad \Gamma_{sf} = \frac{1}{2}T_{\max}(\delta_0-\delta_2).$$

To quantify effects of the cohesive stiffness, the percentage parameter CHE is defined as,

$$\text{CHE}=\Gamma_{hd}/\Gamma.$$

Obviously, for a stiffer cohesive zone CHE is small. For the rigid cohesive zone, CHE=0. For computational investigation we assume a fixed cohesive strength, $T_{\max}=1000$MPa, and the cohesive energy, Γ=100N/mm. To ensure a same softening behavior for all cases, the cohesive softening energy (CSE) will also be fixed as Γ_{sf}=25% Γ=25N/mm. CHE varies from 0 (the rigid cohesive zone) to very soft cohesive zone with Γ_{hd}=25% Γ=25N/mm, i.e. the stiffness of the cohesive zone ψ=20000MPa.

The J_2 flow plasticity is applied with Ramberg-Osgood hardening law as,

$$E\varepsilon = \sigma + \alpha\sigma_0\left(\frac{\sigma}{\sigma_0}\right)^{n}. \quad (6)$$

The material parameters is defined as Young's modulus E=80000MPa; Poisson's ratio ν=0.3; yield stress σ_0=250MPa; $\alpha=1$ and $n=10$.

4. Effects of the cohesive zone stiffness

A compact tension specimen is computationally investigated under plane strain loading conditions with a constant cohesive energy. Fig. 3 shows the force vs. loading line displacement curves from the computations with various cohesive models. The cohesive hardening energy varies from 0 (the rigid cohesive zone) to 25% (a very soft cohesive zone with the stiffness $\psi = E/4$). Generally speaking, the stiffness of the cohesive law arises the specimen resistance and causes higher load. The results confirm, however, that the global reaction of the specimen is not so sensitive to the cohesive law. For CHE<10%, the load-load line displacement curves are numerically independent of variations of the cohesive law.

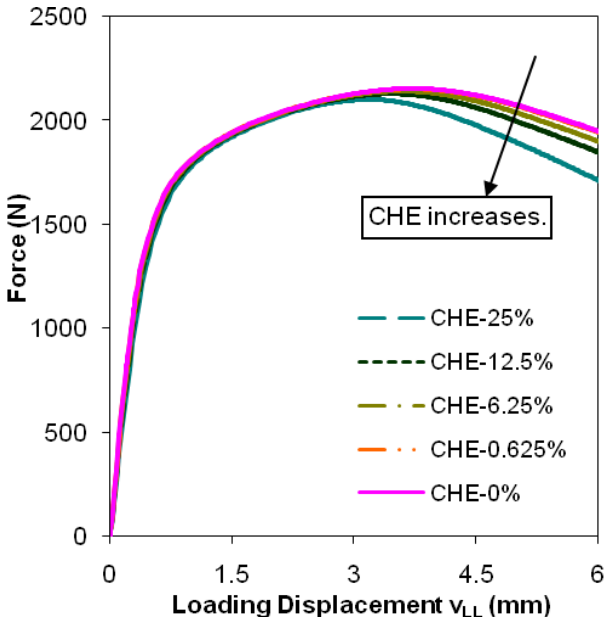

Figure 3. Load vs. loading line displacement for CT specimen using various cohesive laws.

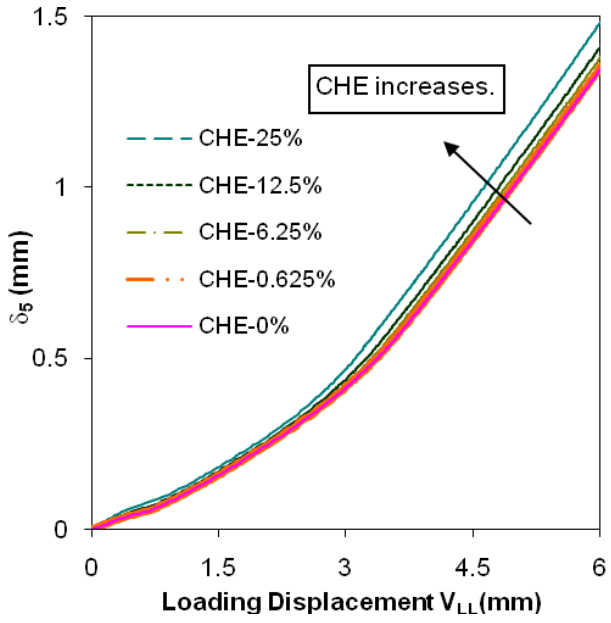

Figure 4. δ_5 vs. loading line displacement for the various cohesive law stiffnesses.

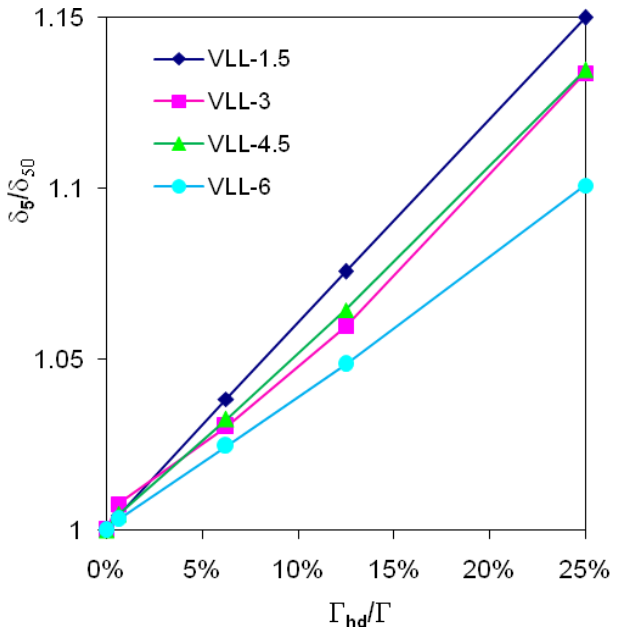

Figure 5. Influence of the cohesive stiffness to the fracture parameter δ_5.

The crack tip opening displacement after Schwalbe et al., δ_5, is documented in Fig. 4 for various cohesive laws. With a softer cohesive law, the δ_5 value becomes larger, as learnt from the figure. Crack initiation approximately occurs at the loading V_{LL}=1.5mm. With increasing loading, the discrepancy between computations grows. More quantified results are presented in Fig. 5. In the figure the deviation of the δ_5 value is summarized for V_{LL}=1.5mm, 3mm, 4.5mm and 6mm, respectively. δ_5 of the rigid cohesive zone is taken as reference. It is clear that the deviation

increase linearly with the CHE and decreased with crack propagation. For the cohesive stiffness $\psi \geq E$, the difference is below 5%.

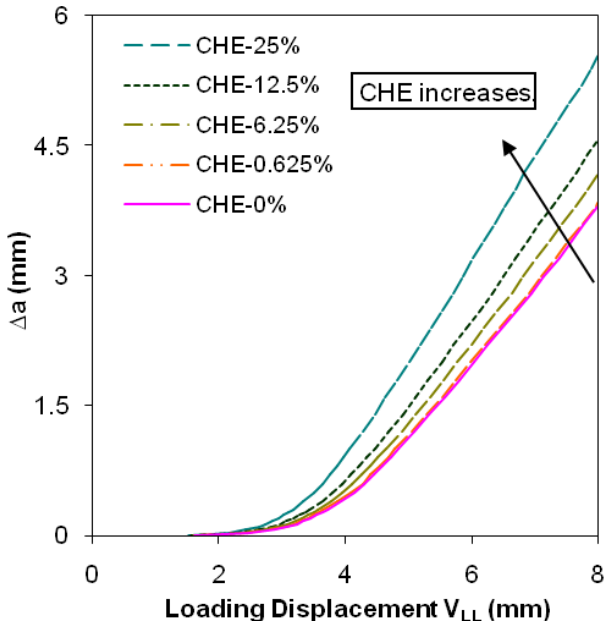

Figure 6. Δa vs. loading line displacement for the various cohesive law stiffnesses.

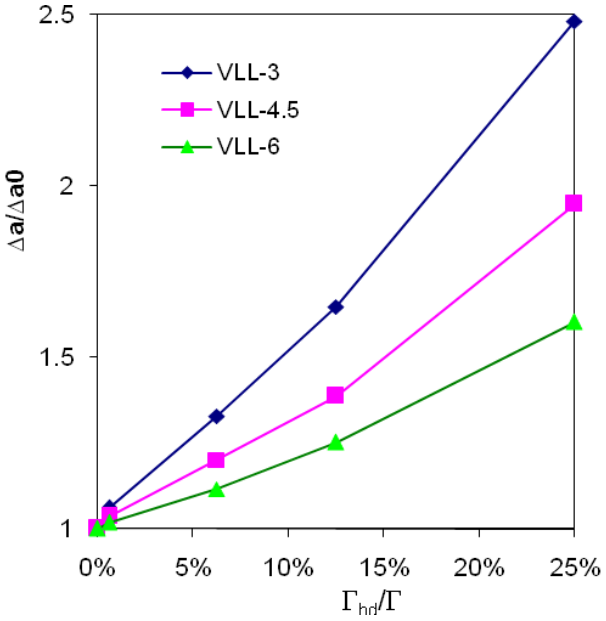

Figure 7. Influence of the cohesive stiffness to the crack propagation Δa.

The cohesive law influences crack propagation in computations. Fig. 6 shows crack growth vs. load line displacement using different cohesive zone stiffnesses. Significant differences of crack growth rate are illustrated in Fig. 6. A gentler cohesive stiffness, which means a higher cohesive hardening energy, leads to a more rapidly crack growth. It is similar to the δ_5 curves. More results are shown in Fig. 7 with crack propagation deviation as a function of load line displacement. The difference of crack growth Δa_0 is taken from the rigid cohesive zone. The figure shows discrepancy as a function of the cohesive stiffness at three different loading stages: V_{LL}=3mm, 4.5mm and 6mm. the results confirm that the predicted crack growth is very sensitive to the cohesive stiffness. For the case with the cohesive stiffness $\psi=E$, the crack growth deviates more 35% from the rigid cohesive model. Generally, the soft cohesive zone model will delay crack propagation in comparing with the rigid cohesive zone model.

5. The energy release rate of fracture at crack initiation

In nonlinear fracture mechanics the energy release rate is introduced as a fracture parameter, which can be evaluated based on the *J*-integral. In FEM the *J*-integral will be calculated based on the virtual crack extension technique [18]. The fracture energy for crack initiation is the far field *J*-integral. Application of the cohesive zone model is based on energy balance around the crack tip. One important question is the relation between Γ and J_i, the *J*-integral value at crack initiation. A common answer is $\Gamma=J_i$ [10,11,12].

Recalling the difference in the cohesive zone modeling, the ductile fracture process should be considered in the ductile traction-separation curve, the cohesive law. During damaging the material around the cohesive zone is plastified and consuming mechanical energy. A crack increment is formed only if the separation reaches δ_0, as shown in Equation (2). The energy dissipation for generating a unit crack increment is the energy release rate. Since the cohesive zone model is describing a continuous damage process, the energy release rate may vary with the cohesive law.

Figure 8 shows variations of the energy release rate at crack initiation, J_i, with the cohesive stiffness, by keeping constant cohesive strength T_{max}. J_i for all considered cohesive laws is larger than the cohesive energy Γ, but decreases monotonically with Γ_{hd}. Since the cohesive strength is generally higher than yield stress of the bulk material. The plastic zone size decreases with Γ_{hd}. In the softening stage of the cohesive law, the bulk material around the crack tip will be elastically unloaded, it leads to plastic energy dissipation. For a soft cohesive zone, the plastic dissipation energy is less than that for a rigid or hard cohesive zone. The fracture energy difference between a rigid cohesive zone and a cohesive zone with the stiffness equal $\psi=E$ is ca. 5%.

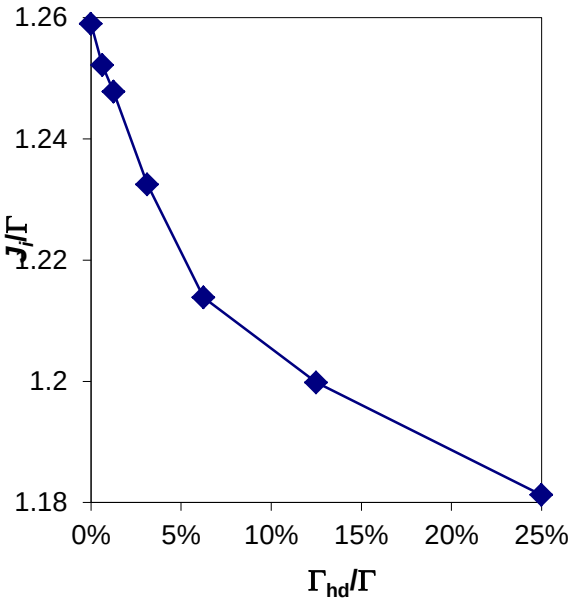

Figure 8. The energy release rate at crack initiation as a function of the cohesive stiffness.

Additionally, the cohesive strength and the curve form may affect the fracture energy in crack simulation. To study effects of the cohesive law systematically, a polynomial cohesive law is defined as

$$T=\begin{cases}\dfrac{27}{4}T_{\max}\dfrac{\delta}{\delta_0}\left(1-\dfrac{\delta}{\delta_0}\right)^2 & \text{for } \delta\le\delta_0,\\ 0 & \text{otherwise.}\end{cases} \qquad (7)$$

The cohesive laws (2) and (7) are plotted in Fig. 9. All curves contain the same cohesive energy of Γ=100N/mm. Two kinds of cohesive laws are studied here. The rigid cohesive zone model (2) contains a constant traction after cohesive zone initiation, whereas the other is a soft cohesive zone model (7). The cohesive strengths are assumed to be $2\sigma_0$ and $5\sigma_0$, respectively. δ_0 is determined for the constant cohesive energy.

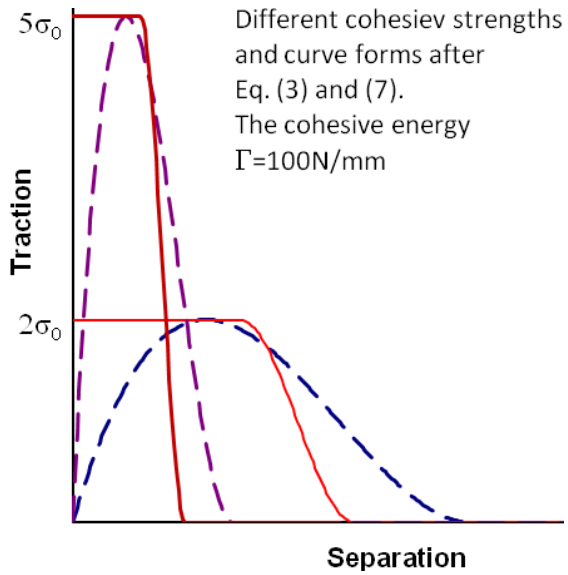

Figure 9. Different cohesive laws used for study fracture energy at crack initiation.

Figure 10 illustrates dependence of the fracture energy at crack initiation on the cohesive law. Only fracture energy release rate for crack initiation is considered. Each point in the figure is a independent computation. For the case with $T_{max}=\sigma_0$, the whole specimen is purely elastic and no plastic dissipation exists, i.e. $J_i=\Gamma$.

With higher T_{max}, the plastic zone around the crack tip grows and elastic unloading becomes more severe. It follows larger plastic dissipation and higher fracture energy since a part of mechanical energy flow into plastification. For high enough T_{max} the plastic energy dissipation reaches a stable value since the plastic zone size becomes constant under given Γ. The critical value

for T_{max} is approximately ca. $3\sigma_0$ for both types of the cohesive laws, which is the most common cohesive strength taken in literature [9,19-22].

Generally speaking, difference between the fracture energy and the cohesive energy is substantial. For $T_{max}>3\sigma_0$, the deviations become stable and reach 30% for the rigid cohesive zone model and 40% for the polynomial soft cohesive zone model. The influence of the cohesive model to the fracture energy is not negligible. To perform a quantitative simulation of cracked specimen, one has to pay attention to postulate the cohesive energy. It is generally smaller than the fracture energy release rate for crack initiation.

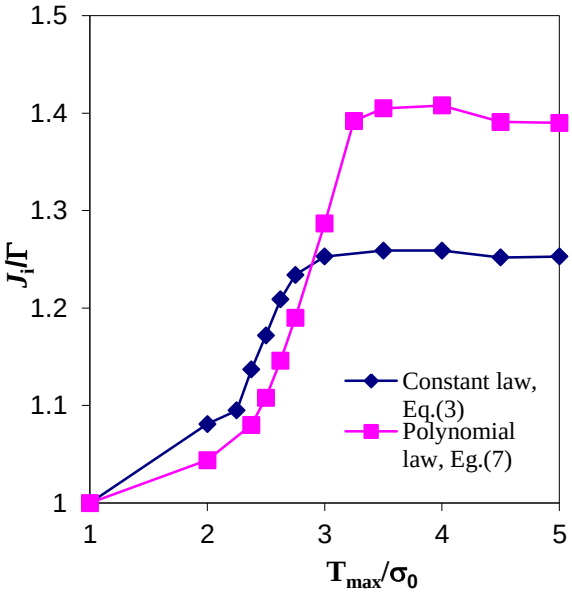

Figure 10. Effects of the cohesive law to the fracture energy at crack initaion.

6. Conclusion

In the present paper two fundamental problems about influence of the cohesive law have been studied from computational aspects: the function form and effects to the fracture energy balance. For this purpose a special cohesive element has been developed and implemented into the commercial FEM code ABAQUS. Computational results confirm following conclusions:

1. Effects of the cohesive zone model with stiffness larger than elasticity modulus ($\psi>E$) are negligible in the load vs. load line displacement curve. However, influence to the fracture parameter, such as δ_5, is ca. 5%. The soft cohesive zone model generates higher δ_5 value.
2. In prediction of the crack propagation amount the cohesive stiffness becomes more important. The Δa deviations among models for $\psi \geq E$ reach 35%. To obtain a realistic crack propagation, one has to increase the stiffness of the cohesive zone.
3. The fracture energy release rate from the cohesive zone model computation is not equal to the cohesive energy. The difference depends on the cohesive law and vanishes only in an elastic specimen. With increasing cohesive strength, the discrepancy between them grows and becomes stable for $T_{max}>3\sigma_0$ under plane strain loading conditions. The maximum deviation exceeds 40%.

References

[1] J.W. Hutchinson, A.G. Evans. *Mechanics of Materials*, 48 (2000) 125-135.
[2] Y.J. Xu, H. Yuan. Engineering Fracture Mechanics 78 (2011) 544-558.
[3] C.R.Chen, O.Kolednik. *International Journal of Fracture*, 132 (2005) 135-152
[4] Z.H.Jin, C.T.Sun. *International Journal of Fracture*, 134 (2005) 91-108.
[5] C.R.Chen, O.Kolednik. *International Journal of Fracture*, 132 (2005) 135-152.
[6] K.H.Schwable, I.Scheider, A.Cornec. The SIAM method for applying cohesive models to damage behavior of engineering materials and structures. GKSS Technical Report (2009) ISSN 0344-9629.
[7] A.Needleman. *Journal of Applied Mechanics*, 54 (1987) 525-531.
[8] A.Needleman. *International Journal of Fracture*, 42 (1990) 21-40.
[9] V. Tvergaard, J.W. Hutchinson. *Journal of the Mechanics and Physics of Solids*, 40 (1992) 1377-1397.

[10] I.Scheider, W.Brocks. *Engineering Fracture Mechanics*, 70 (2003) 1943-1962.
[11] G.Lin, A.Cornec, K.H.Schwable. *Fatigue and Fracture of Engineering Materials and Structures*, 21 (1998) 1159-1173.
[12] H.Yuan, G.Y.Lin, A.Cornec. *Journal of Engineering Materials and Technology*, 118 (1996) 192-200.
[13] H.Yuan, J.Chen, K.Krompholz, F.H.Wittmann. *Computational Materials Science*, 26 (2003) 230-243.
[14] C.R.Chen, O.Kolednik, I.Scheider, T.Siegmund, A.Tatschl, F.D.Fisher. *International Journal of Fracture*, 120 (2003) 517-536.
[15] Y.J.Xu, H.Yuan. *Computational Material Science*, 46 (2009) 579-585.
[16] D. Gross, T. Seelig. *Fracture Mechanics: With an Introduction to Micromechanics*. 2nd Edition. Springer Verlag, Berlin, 2010.
[17] T.R.Chandrupatla, A.D.Belegundu. *Introduction to Finite Elements in Engineering*. 3rd Edition, Prentice-Hall, 2002.
[18] ABAQUS Version 6.10, ABAQUS Inc., U.S.A. 2011.
[19] L.Xia, S.F.Shih. *Journal of Mechanics and Physics Solids*, 43 (1995) 233-259.
[20] L.Xia, S.F.Shih. *Journal of Mechanics and Physics Solids*, 43 (1995) 1953-1981.
[21] V. Tvergaard, J.W. Hutchinson. *International Journal of Solids and Structures*, 33 (1996) 3297-3308.
[22] T.Siegmund, W.Brocks. *International Journal of Fracture*, 99 (1999) 97-116